



A Journal of the Gesellschaft Deutscher Chemiker

# Angewandte Chemie

GDCh

International Edition

www.angewandte.org

## Accepted Article

**Title:** Controlling Ultra-Large Optical Asymmetry in Amorphous Molecular Aggregations

**Authors:** Liangliang Zhu, Bin Wu, Hongwei Wu, Yunyun Zhou, Dongxiao Zheng, Xiaoyong Jia, and Lei Fang

This manuscript has been accepted after peer review and appears as an Accepted Article online prior to editing, proofing, and formal publication of the final Version of Record (VoR). This work is currently citable by using the Digital Object Identifier (DOI) given below. The VoR will be published online in Early View as soon as possible and may be different to this Accepted Article as a result of editing. Readers should obtain the VoR from the journal website shown below when it is published to ensure accuracy of information. The authors are responsible for the content of this Accepted Article.

**To be cited as:** *Angew. Chem. Int. Ed.* 10.1002/anie.202012224

**Link to VoR:** <https://doi.org/10.1002/anie.202012224>

# Controlling Ultra-Large Optical Asymmetry in Amorphous Molecular Aggregations

Bin Wu, Hongwei Wu, Yunyun Zhou, Dongxiao Zheng, Xiaoyong Jia, Lei Fang and Liangliang Zhu\*

**Abstract:** Although ultra-large optical asymmetry appears in crystalline materials, distractions from the mesoscopic ordering often causes inauthenticity in chiropticality. In addition, the formation and maintenance of crystalline states require complicated technical efforts. In amorphous materials, however, it remained challenging and elusive to achieve large chiropticality, not to mention the control of the degree of asymmetry. Herein, we report the quantitative control of chiral amplification, on amorphous supramolecular structures of cholesterol-linked bis(dipyrrinato)zinc(II), to an exceptionally high level. The amorphous molecular aggregations of these complex building blocks exhibit mirror-image chiropticality. A proper chiral packing of the building block at several molecular scale contributes considerably to the absorptive dissymmetry factor  $g_{\text{abs}}$ , although the system is overall disordered. The intense and tunable aggregation strength renders a variable  $g_{\text{abs}}$  value up to +0.10 and +0.31 in the solution and in film state, higher than those observed in most previously reported cases. On this basis, a superior ON-OFF switching of chiropticality is realized under external stimuli. By eliminating the demand on material crystallinity, this work establishes a general design principle to control over ultra-large optical asymmetry on a wider scope of chiral materials.

## Introduction

Chiral amplification is an appealing characteristic in numerous natural hierarchical architectures and living helical systems.<sup>1</sup> In particular, chiral amplification by chiral self-assembly of building blocks into artificial nanostructures shows promising potentials in materials science and optoelectronics.<sup>2</sup> So far, ultra-large optical asymmetry (e.g., an absorptive dissymmetry factor  $g_{\text{abs}} > 0.1$ ) on the basis of crystalline building blocks have been reported,<sup>3</sup> which connects to the further development of asymmetric photocatalysis, circularly polarized luminescence, or even circular dichroism based imaging techniques. However, these chiroptical signals can be easily affected by other interfering factors (e.g., linear polarization), and the emerged circular dichroism (CD) signals are not necessarily magneto-electric-dependent.<sup>4</sup> In addition, molecular configuration responsible for the ultra-large optical asymmetry in these crystalline states is

quite restricted. Conversely, it is essential to control the chiral amplification in amorphous materials, because such systems do not have limitations in maintaining the mesoscopic ordering. Moreover, as compared to the crystalline materials that are relatively inflexible, stimuli response can be expected in the amorphous systems with high chiroptical signal tunable. Nevertheless, it is challenging to engineer an ultra-large optical asymmetry in amorphous molecular aggregations, probably due to the difficulty of enhancing aggregation strength by the cooperation of different chiral packing modes.<sup>5</sup>

To address this issue, a possible strategy is to enroll strong chiral packing components together with flexible and controllable linkers. In this way, chiral packing of the building block at several molecular scale may contribute considerably to  $g_{\text{abs}}$ , leaving the system overall amorphous. Chiral coordinated supramolecules have been receiving considerable attention owing to their strong complexation interaction in building materials.<sup>6</sup> Among various ligands, dipyrin, which can accept a wide variety of metal ions to form bis(dipyrrinato)metal(II) complexes, has been regarded as a promising candidate for the construction of different supramolecular structures.<sup>7</sup> On the other hand, cholesterol can effectively drive self-assemblies for supramolecular chirality. The unique chiral packing ability of cholesterol is derived from weak van der Waals interactions, which make it useful and smart for the construction of nanostructures with aggregation strength and morphology tunable.<sup>8</sup> Inspired by these structural factors, instead of the routine doping strategy within a framework or polymers for preparing amorphous materials,<sup>9</sup> we synthesized a big and staggered complex building block to minimize the crystalline properties, but a strong and tunable chirality driving force is still included. Thus, the possible asymmetry control in the interim may facilitate chirality amplification upon an amorphous molecular aggregation.

Therefore, we present a cholesterol-conjugated bis(dipyrrinato)zinc(II) molecule (compound **ZnL2-1**, see Figure 1), which was prepared through the accurate complexation of the ligand (compound **L-1**) with the zinc(II) ion, to serve as a highly efficient chiral building block (see synthetic route for the preparation of these compounds in Figure S1). Analogous **ZnL2-2** and **ZnL2-3** were synthesized as reference molecules for control studies to better clarify the mechanism of the controlled amplification of supramolecular chirality. We determined that a decrease in the ratio of benign cosolvents in mixed solutions can cause the quantitative enhancement of the asymmetry degree, up to an extremely high absorptive dissymmetry factor; these values are larger than those observed in most previously reported cases of supramolecular chirality.<sup>10</sup> The asymmetry can be further improved by an increase in the enantiomeric excess with the dynamic transfer of the aggregates. These studies can verify the key role of aggregation strength in chiral amplification. In addition, external stimulus, film grinding, was also employed as an *in situ* tuning way to allow the reversible ON-OFF switching of ultra-large chiropticality in the solid state, on the basis of the unique chiral packing and dissociation under external stimuli.

[a] Mr. B. Wu, Dr. Y. Zhou, Mr. D. Zheng, Prof. Dr. L. Zhu  
State Key Laboratory of Molecular Engineering of Polymers  
Department of Macromolecular Science  
Fudan University, Shanghai 200438, China  
E-mail: zhuliangliang@fudan.edu.cn

[b] Dr. H. Wu  
College of Chemistry, Chemical Engineering and Biotechnology  
Donghua University, Shanghai 201620, China

[c] Dr. X. Jia  
Henan Key Laboratory of Photovoltaic Materials  
Henan University, Kaifeng 475004, China

[d] Prof. Dr. L. Fang  
Department of Chemistry  
Texas A&M University, 3255 TAMU, College Station, Texas 77843,  
United States

Supporting information for this article is given via a link at the end of the document.

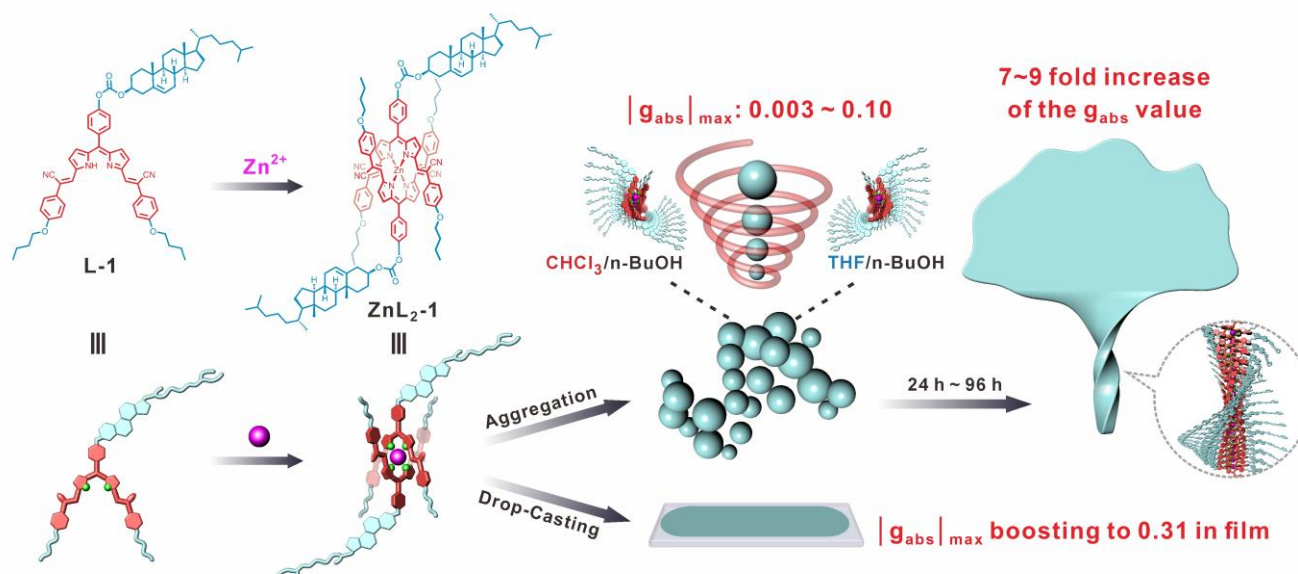


**Figure 1.** Chemical structure of L-1 and ZnL<sub>2</sub>-1, and their cartoon illustration of the amorphous chiral molecular aggregations and the chirality-controlled amplification to an exceptionally high level.

## Results and Discussion

### Supramolecular Chirality upon Amorphous Aggregations.

To promote the molecular aggregation of the building block, we explored the addition of different stock solutions of ZnL<sub>2</sub>-1 to a poor solvent. By optimization, perfect mirror-image chiroptical signals of ZnL<sub>2</sub>-1 can be exhibited in CHCl<sub>3</sub>/n-BuOH and THF/n-BuOH mixed solution (Figure 2), as the CD signal of the supramolecular architecture with a cholesterol based building block is always solvent selective.<sup>11</sup> As the absorption of a chiral cholesterol unit is below 250 nm, the CD signals observed in the visible spectral region are from the supramolecular chirality of the bis(dipyrrinato)zinc(II) skeleton, which originated from the chiral molecular arrangement in different clockwise fashions. In addition, the results reflected the packing capability of the complex building block, whereas its precursor L-1 does not have a chiroptical signal under the same solvent condition despite having a similar absorbance (Figure S2).

When the stock solutions of ZnL<sub>2</sub>-1 (2 mM, every batch of 5  $\mu$ L in CHCl<sub>3</sub> or THF as the benign cosolvent) were titrated into poor solvent n-BuOH, CD signals increased in a stepwise manner (Figure 2b). The X-ray diffraction (XRD) patterns of the ZnL<sub>2</sub>-1 aggregates prepared from the mixed solutions are broad

and do not exhibit peaks of the raw sample (Figure S3). This result indicates that such a chiral molecular aggregation resulted in an amorphous state.

A geometric optimization for the bis(dipyrrinato)zinc(II) moiety shows that both ligands are located orthogonally in the complex (Figure S4). This probably explains an anti-crystalline property of the building block during molecular aggregations. The amorphous information of ZnL<sub>2</sub>-1 can be further referenced by morphological study. The SEM analysis showed that molecular aggregation occurred, and the sample from both mixed solutions showed a randomly dispersed beads-string morphology (see a typical image in Figure 2c) instead of a well-known regular helical morphology. These results suggested that in such supramolecular structures, supramolecular chirality was derived only from the chiral packing of the building block at several molecular scale (as illustrated in Figure 2a).<sup>9b,12</sup> Meantime, the random morphology also explains the overall amorphous characteristic of the system. The absorptive dissymmetry factor  $g_{abs}$ , which is defined by the ratio of CD intensity to the corresponding absorption (see Supplemental Information), remained at the same level upon the cosolvent titration despite an increase in the concentration of ZnL<sub>2</sub>-1 (Figures 2d and 2e), which indicated that the degree of asymmetry was independent of the final concentration of ZnL<sub>2</sub>-1.

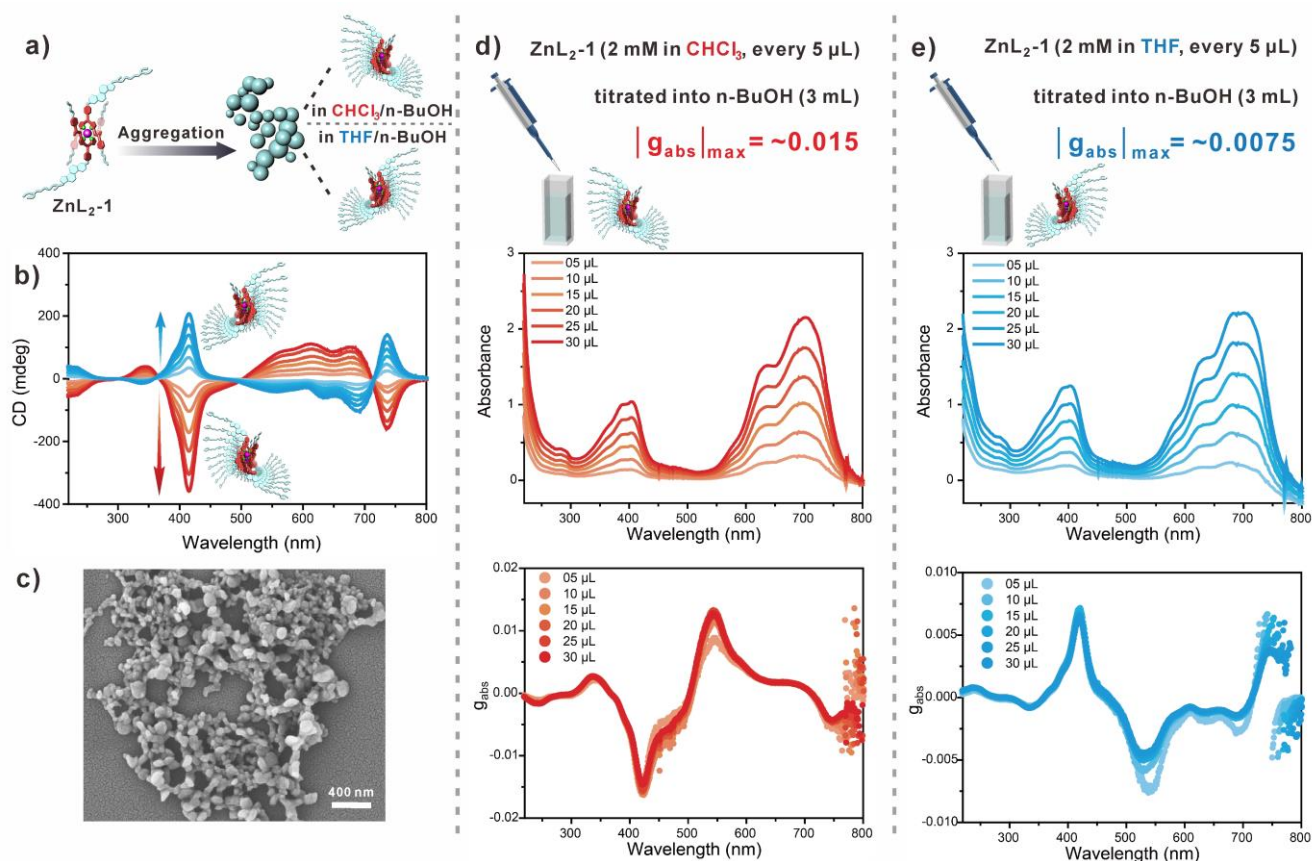


**Figure 2.** Supramolecular Chirality upon Amorphous Aggregations. a) Illustration of chiral self-assembly. b) CD spectra of **ZnL<sub>2</sub>-1** in  $\text{CHCl}_3/n\text{-BuOH}$  (red lines) and  $\text{THF}/n\text{-BuOH}$  (blue lines) mixtures with the titration of stock solutions (2 mM, every batch of 5  $\mu\text{L}$  in  $\text{CHCl}_3$  or  $\text{THF}$  as a cosolvent) into  $n\text{-BuOH}$  (3 mL). c) A typical SEM image of **ZnL<sub>2</sub>-1** prepared from the  $\text{CHCl}_3/n\text{-BuOH}$  mixture. d, e) Corresponding UV-Vis and  $g_{\text{abs}}$  spectra of **ZnL<sub>2</sub>-1** upon  $\text{CHCl}_3$  (d) and  $\text{THF}$  (e) cosolvent titration.

**Quantitative Control of the Asymmetry Degree.** Next, we explore the effect of stock solution fraction in the mixed solution of **ZnL<sub>2</sub>-1**. Similar to the case in the cosolvent titration experiment, the mirror-image CD signals sharply increased (and showed a prominent ellipticity of more than  $-1000$  mdeg) along with a decrease in the benign cosolvent ratio (the final concentration of 20  $\mu\text{M}$  was maintained in a cosolvent/ $n\text{-BuOH}$  mixed solution with  $v/v = 1.0, 0.5, 0.25,$  and  $0.125 : 100$ , Figure 3). The values in the UV-Vis spectra slightly decreased with a decrease in the cosolvent ratio, which suggested a possible change of aggregation strength of **ZnL<sub>2</sub>-1** rather than a change of the final concentration of **ZnL<sub>2</sub>-1**. Interestingly, the absolute value of  $g_{\text{abs}}$  of both mixed solutions was considerably enhanced with the decrease in the cosolvent ratio (see the  $g_{\text{abs}}$  spectra in Figure 3), which differs from the relatively stationary behavior of  $g_{\text{abs}}$  shown in Figure 2. These results illustrated the importance of aggregation strength on tuning the asymmetry degree, whereas the creation of more aggregates is not useful.

An increase in the aggregation strength is further confirmed by the morphological study (see SEM images in Figures 3c and 3d). The beads-string structures produced using the cosolvent/ $n\text{-BuOH}$  ratio of 1.0:100 appeared to be more delicate with a

cross-sectional diameter of 30–40 nm, whereas stepwise-produced structures became thicker with a cross-sectional diameter of 200–300 nm when they were produced using the cosolvent/ $n\text{-BuOH}$  ratio of 0.125:100. This result is an apparent reflection of the increase in aggregation intensity of **ZnL<sub>2</sub>-1**. By the treatment under a very selective solvent condition (see Supplemental Information), we can even perform a single crystal characterization on **ZnL<sub>2</sub>-1**. Figure S5 shows the couples of different short contacts can be labelled in the packing structure of **ZnL<sub>2</sub>-1**, and a quite small packing distance is found (3.29 Å), which is typically smaller than the routine packing distance of organic  $\pi$ -skeletons (3.4–3.8 Å). This indicates the self-assembly ability of **ZnL<sub>2</sub>-1** upon the unique structural design and may also explain the high aggregation strength. There is no shift trend of the peaks in FT-IR spectra among different samples of **ZnL<sub>2</sub>-1** (Figure S6), featuring that the aggregation strength change is basically accompanied by molecular packing rather than some special non-covalent bonds. Furthermore, linear relationships are observed between the  $\log |g_{\text{abs}}|_{\text{max}}$  value and the  $\log$  cosolvent ratio (see the insets in the  $g_{\text{abs}}$  spectra in Figures 3a and 3b), featuring a quantitative control of chiral amplification.

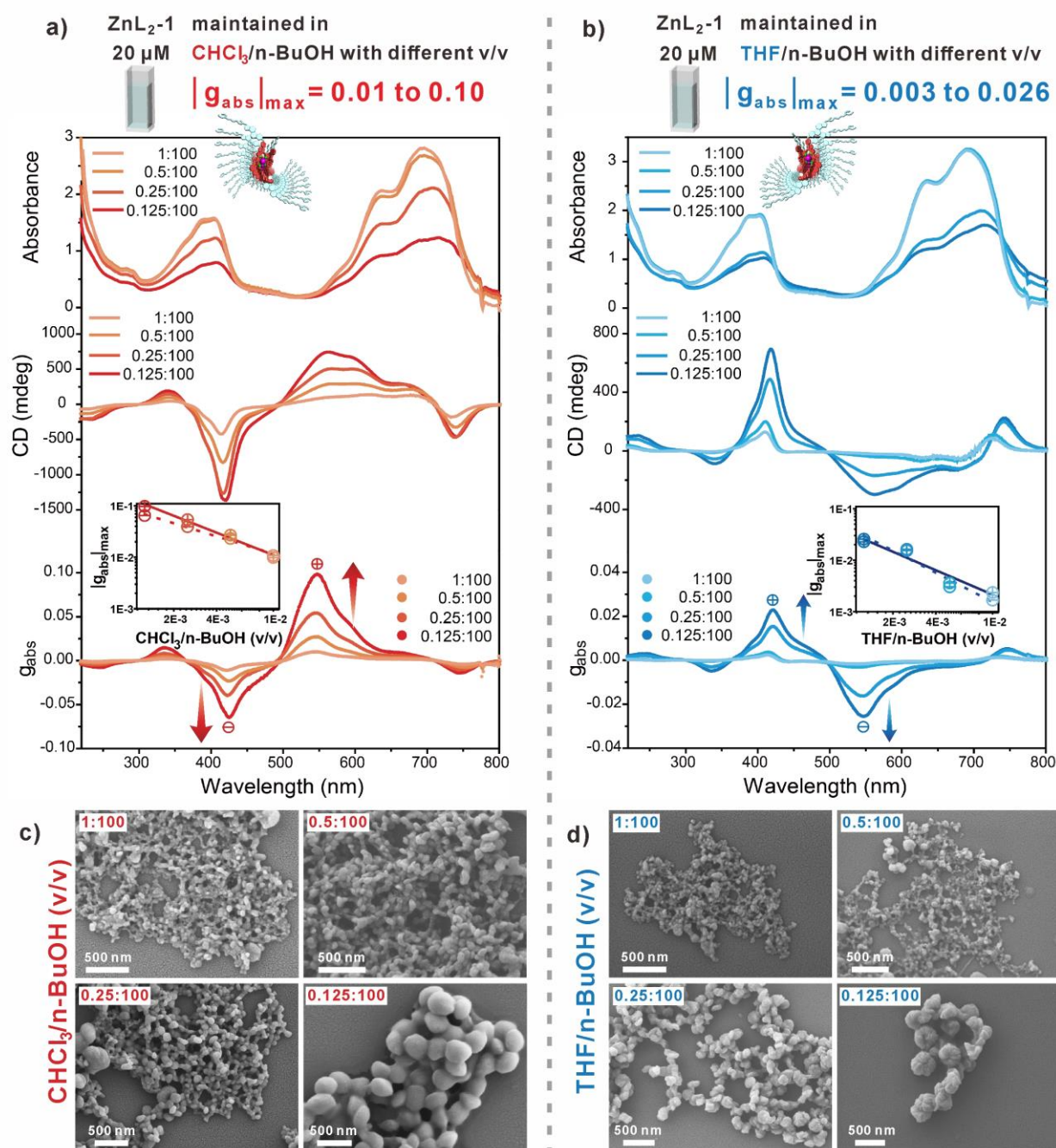


**Figure 3.** Quantitative Control of the Asymmetry Degree. a, b) UV-Vis, CD, and  $g_{abs}$  spectra of **ZnL<sub>2</sub>-1** with a decrease in the CHCl<sub>3</sub> (a) and THF (b) cosolvent ratio (the final concentration of 20  $\mu$ M was maintained in the cosolvent/n-BuOH mixed solution with v/v = 1.0, 0.5, 0.25, and 0.125:100). Insets: plots of  $|g_{abs}|_{max}$  vs. the cosolvent/n-BuOH ratio. c, d) SEM images of **ZnL<sub>2</sub>-1** prepared from CHCl<sub>3</sub>/n-BuOH (c) and THF/n-BuOH (d) mixed solution with v/v = 1.0, 0.5, 0.25, and 0.125:100.

**Further Improving Asymmetry Degree by Aggregation Dynamic Transfer.** Subsequent to exploring the initial self-assembly stage of **ZnL<sub>2</sub>-1** in cosolvent/n-BuOH mixed solutions, we discovered a spontaneous dynamic transfer in the supramolecular structures.<sup>13</sup> Surprisingly, mirror-image CD signals gradually produced a spectrum with the same peak shape and sign after 24–96 h of aging (Figures 4a and 4b). This result indicates that even different clockwise directions exist in

cholesterol-driven chiral packing,<sup>14</sup> and only one final supramolecular structure with a minimum energy can be observed.<sup>15</sup> The SEM analysis shows that the initial beads-string morphologies underwent a dynamic transfer and finally yielded a unique leaf-like morphology (Figures 4c and 4d). This morphology revealed a clear helicity characteristic, which provided a visualization effect for the chiral packing of the building block from the molecular to mesoscopic level.

In accordance with the CD signal variation, the  $g_{\text{abs}}$  spectra were also converted into the final state along with the aggregation dynamic transfer (Figure S7). During this process, a further improvement in the asymmetry degree (a 7–9 fold increase in the  $g_{\text{abs}}$  value) can be seen. We attribute this to an increase in the enantiomeric excess in the chiral packing, whereas the leaf-like morphology with a *P*-helicity of nearly 100% can be monitored through a series of statistical SEM observations with a large number of samples (*i.e.*, no structures with *M*-helicity are observed, Figures S8 and S9). Furthermore, the dynamic transfer is cosolvent ratio-dependent. The smaller the cosolvent ratio was, the more difficult was it to change the aggregation structure (see Figure S10). This implies the effect of aggregation strength-induced morphological locking.

Molecular structure is an internal factor that controls the molecular aggregation behaviors. In this study, another two reference building blocks (*i.e.*, **ZnL<sub>2</sub>-2** with a carbamate group connecting cholesterol and the chromophore moiety and **ZnL<sub>2</sub>-3** with an additional alkyl spacer attached) were synthesized for the control study (see structures and cartoon illustration in Figure S11). Parallel experiments were conducted under the same condition of the cosolvent fraction ratio (cosolvent/*n*-BuOH, 30  $\mu$ L/3 mL; 20  $\mu$ M). CD spectra (Figure S12) and SEM

images (Figure S13) show that the aggregation of **ZnL<sub>2</sub>-2** remained constant with a relatively low optical asymmetry and  $g_{\text{abs}}$  value, indicating that the introduction of hydrogen bonding weakens the aggregation strength (see also a H-bonding verification of **ZnL<sub>2</sub>-2** in FT-IR spectra, Figure S14). In contrast, although **ZnL<sub>2</sub>-3** can undergo a dynamic transfer in the aggregation, as confirmed by the CD spectra and morphological change (Figures S15 and S16), the supramolecular structure was only translated into larger particle aggregates composed of rhombic nanoflakes, which was probably owing to the relatively loose molecular packing (circumstantially evidenced by a more amorphous characteristic of **ZnL<sub>2</sub>-3** in the XRD patterns, Figure S17). For better comparison, the different self-assembled patterns were illustrated in Figure S11. In addition, we found that only *n*-BuOH as the poor solvent could facilitate the mirror-image optical performance of **ZnL<sub>2</sub>-1** (Figure S18). This phenomenon may be ascribed to the contribution of the interaction between the butoxyl group in **ZnL<sub>2</sub>-1** and the poor solvent *n*-BuOH. These discussions allow us to conclude that the unique structural design (including the linker design) of **ZnL<sub>2</sub>-1** is advantageous for the existence of strong chiral packing and the overall disorder, favorable for modeling and visualizing a chiral amplification.

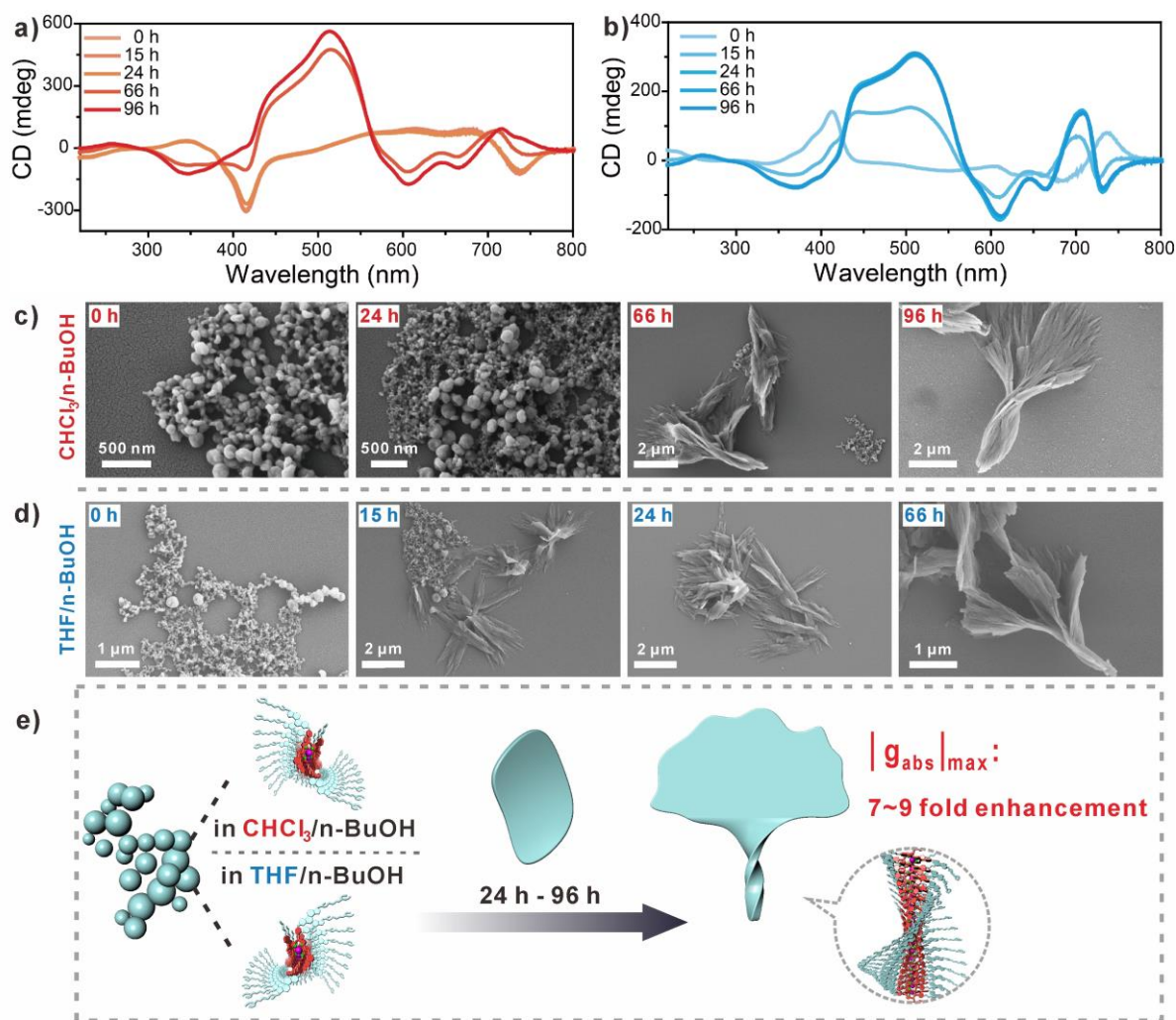


**Figure 4.** Further Improving Asymmetry Degree by Aggregation Dynamic Transfer. a, b) Time-dependent CD spectra of **ZnL<sub>2</sub>-1** (20  $\mu$ M) in  $\text{CHCl}_3/n\text{-BuOH}$  (a) and  $\text{THF}/n\text{-BuOH}$  (b; cosolvent/ $n\text{-BuOH}$  = 1:100, v/v) with 24–96 h aging. c, d) SEM images of **ZnL<sub>2</sub>-1** prepared from a  $\text{CHCl}_3/n\text{-BuOH}$  (c) and  $\text{THF}/n\text{-BuOH}$  (d) mixed solution with different aging time. e) Schematic representation of the self-assembly dynamic transfer process.

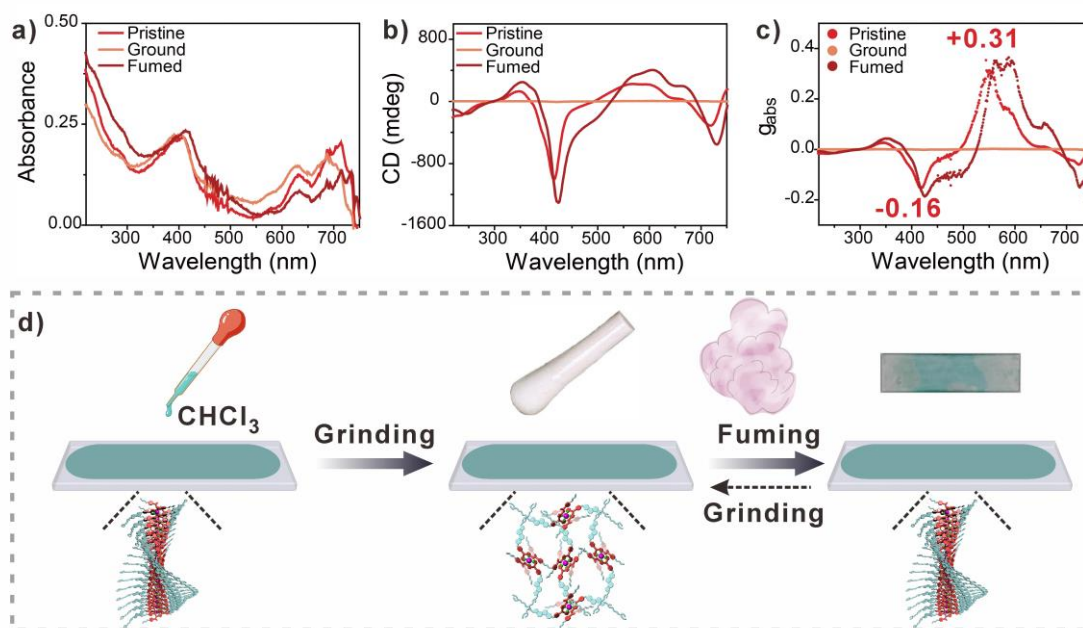


**Figure 5.** ON-OFF Chiral switching. a-c) UV-Vis (a), CD (b) and the corresponding  $g_{\text{abs}}$  (c) spectra of the pristine, ground and fumed films that were drop-cast with a **ZnL<sub>2</sub>-1** stock solution in  $\text{CHCl}_3$ . d) Schematic representation of the chiral switching process.

**ON-OFF Chiral Switching in the Film State.** It has been reported that  $g_{\text{abs}}$  values in organic matter thin films are typically in the range of  $10^{-4}$ – $10^{-2}$ .<sup>16</sup> Only in rare cases,  $g_{\text{abs}}$  values can exceed 0.3 or even 1 such as in some crystalline thin films.<sup>17</sup> As shown in Figure 5, a film was formed by the evaporation of **ZnL<sub>2</sub>-1** in a  $\text{CHCl}_3$  stock solution cast on a quartz plate. The film showed extremely high  $g_{\text{abs}}$  values (reaching  $-0.16$  and  $+0.31$  at the wavelengths of 418 nm and 550 nm, respectively), which were comparable to the reported case with an ultra-large optical asymmetry. Such a giant value can be regarded as the ultimate case while the ratio of benign cosolvent is reduced to zero. The disturbance by any possible linear dichroism artifacts in our case can be negligible (see Figure S19 ~ S21). In addition, the pristine CD curve of the **ZnL<sub>2</sub>-1** film was similar to that of corresponding aggregates in the  $\text{CHCl}_3/n\text{-BuOH}$  mixture at the early stage. The CD and asymmetric signals could completely vanish subsequent to grinding, which suggested the dissociation of chiral packing under an external force stimulus (see Figures 5b and 5c). Interestingly, such a grinding induced chiral silence could be restored subsequent to the sample being fumed in a  $\text{CHCl}_3$  vapor, which indicated that the chiral packing was regenerated in the film state. The reversible chiral conversion exhibited a successful ON-OFF switching for the ultra-large optical asymmetry by an *in situ* tuning way.

Of course, all the aggregated solution systems or films are amorphous, verified by the lack of signal both in XRD and small angle X-ray scattering (SAXS) spectra (Figures S22 and S23). All these results suggest such an ultra-large optical asymmetry in this system is essentially from the chiral packing of the building block at several molecular scale with an extremely high and tunable aggregation strength. An explicit comparison with

previous results (Table S1) shows that our system is competitive with the previous results. This fact also reflects that such a tuning of ultra-large optical asymmetry is more meaningful from the perspective of the material universality, on the basis of which the stimuli response can be more readily achieved. The CD and corresponding  $g_{\text{abs}}$  value of **ZnL<sub>2</sub>-1** crystal or powder were much smaller than those of the amorphous counterpart in aggregation or film state (Figure S24). This further shows the advantage of the amorphous aggregation.

## Conclusion

In summary, we successfully demonstrated a strategy for the control of ultra-large optical asymmetry in amorphous molecular aggregation on the basis of a cholesteryl-linked bis(dipyrrinato)zinc(II) complex building block, where the existence of strong chiral packing components and the flexible linker played a key role. A proper chiral packing of the building block at several molecular scale contributes considerably to  $g_{\text{abs}}$ , leaving the system overall disordered. It was determined that the aggregation strength rather than the final concentration was essential in tuning the asymmetry degree. Meanwhile, asymmetry could be further improved by an increase in enantiomeric excess with the dynamic transfer of the supramolecular structures. We emphasize that  $g_{\text{abs}}$  can be stepwise tuned into an ultra-large value, which shows a considerable potential for versatile chiral applications including the switchable chiropticity in the solid state upon external stimuli. We believe that this strategy of the quantitative engineering of ultra-large optical asymmetry in amorphous aggregations opens

a way towards chirality-controlled amplification at a more general scale of materials.

## Acknowledgements

This work was supported by 2019 NSFC (21975046), and partially from the National Key Research and Development Program of China (2017YFA0207700).

**Keywords:** chirality • supramolecular aggregation • ultra-large optical asymmetry • helicity • ON-OFF chiral switch

- [1] a) B. J. Pieters, M. B. van Eldijk, R. J. Nolte, J. Mecnovic, *Chem. Soc. Rev.* **2016**, *45*, 24-39; b) S. Zhang, *Nat. Biotechnol.* **2003**, *21*, 1171-1178; c) E. Yashima, N. Ousaka, D. Taura, K. Shimomura, T. Ikai, K. Maeda, *Chem. Rev.* **2016**, *116*, 13752-13990; d) M. Li, L.-J. Chen, Y. Cai, Q. Luo, W. Li, H.-B. Yang, H. Tian, W.-H. Zhu, *Chem* **2019**, *5*, 634-648.
- [2] a) O. Dumele, J. Chen, J. V. Passarelli, S. I. Stupp, *Adv. Mater.* **2020**, e1907247; b) Y. Sang, J. Han, T. Zhao, P. Duan, M. Liu, *Adv. Mater.* **2019**, e1900110; c) W. Ma, C. Hao, M. Sun, L. Xu, C. Xu, H. Kuang, *Mater. Horiz.* **2018**, *5*, 141-161; d) Z. Shen, Y. Sang, T. Wang, J. Jiang, Y. Meng, Y. Jiang, K. Okuro, T. Aida, M. Liu, *Nat. Commun.* **2019**, *10*, 3976; e) B. Sun, Y. Kim, Y. Wang, H. Wang, J. Kim, X. Liu, M. Lee, *Nat. Mater.* **2018**, *17*, 599-604; f) F. Wang, C. L. Feng, *Angew. Chem. Int. Ed.* **2018**, *57*, 5655-5659.
- [3] a) S. Furumi, Y. Sakka, *Adv. Mater.* **2006**, *18*, 775-780; b) R. K. Vijayaraghavan, S. Abraham, H. Akiyama, S. Furumi, N. Tamaoki, S. Das, *Adv. Funct. Mater.* **2008**, *18*, 2510-2517; c) B. A. San Jose, J. Yan, K. Akagi, *Angew. Chem. Int. Ed.* **2014**, *53*, 10641-10644.
- [4] M. Schulz, J. Zablocki, O. S. Abdullaeva, S. Bruck, F. Balzer, A. Lutzen, O. Artega, M. Schiek, *Nat. Commun.* **2018**, *9*, 2413.
- [5] a) M. Liu, L. Zhang, T. Wang, *Chem. Rev.* **2015**, *115*, 7304-7397; b) C. Roche, H. J. Sun, P. Leowanawat, F. Araoka, B. E. Partridge, M. Peterca, D. A. Wilson, M. E. Prendergast, P. A. Heiney, R. Graf, H. W. Spiess, X. Zeng, G. Ungar, V. Percec, *Nat. Chem.* **2016**, *8*, 80-89; c) H. Wu, Y. Zhou, L. Yin, C. Hang, X. Li, H. Agren, T. Yi, Q. Zhang, L. Zhu, *J. Am. Chem. Soc.* **2017**, *139*, 785-791; d) P. Xing, Y. Li, S. Xue, S. Z. Fiona Phua, C. Ding, H. Chen, Y. Zhao, *J. Am. Chem. Soc.* **2019**, *141*, 9946-9954; e) G. Liu, J. Sheng, H. Wu, C. Yang, G. Yang, Y. Li, R. Ganguly, L. Zhu, Y. Zhao, *J. Am. Chem. Soc.* **2018**, *140*, 6467-6473.
- [6] a) L. J. Chen, H. B. Yang, M. Shionoya, *Chem. Soc. Rev.* **2017**, *46*, 2555-2576; b) Y. Sun, S. Li, Z. Zhou, M. L. Saha, S. Datta, M. Zhang, X. Yan, D. Tian, H. Wang, L. Wang, X. Li, M. Liu, H. Li, P. J. Stang, *J. Am. Chem. Soc.* **2018**, *140*, 3257-3263; c) W. Feng, J. Y. Kim, X. Wang, H. A. Calcaterra, Z. Qu, L. Meshi, N. A. Kotov, *Sci. Adv.* **2017**, *3*, e1601159; d) A. Gansäuer, I. Winkler, T. Klawonn, R. J. M. Nolte, M. C. Feiters, H. G. Börner, J. Hentschel, K. H. Dötz, *Organometallics* **2009**, *28*, 1377-1382; e) J. Jiang, Y. Meng, L. Zhang, M. Liu, *J. Am. Chem. Soc.* **2016**, *138*, 15629-15635; f) S. Kawano, N. Fujita, S. Shinkai, *J. Am. Chem. Soc.* **2004**, *126*, 8592-8593; g) L. Zhu, X. Li, S. Wu, K. T. Nguyen, H. Yan, H. Agren, Y. Zhao, *J. Am. Chem. Soc.* **2013**, *135*, 9174-9180; h) H. Wang, W. Zhu, J. Li, T. Tian, Y. Lan, N. Gao, C. Wang, M. Zhang, C. F. J. Faul, G. Li, *Chem. Sci.* **2015**, *6*, 1910-1916.
- [7] a) S. A. Baudron, *Dalton Trans.* **2013**, *42*, 7498-7509; b) R. Sakamoto, T. Iwashima, M. Tsuchiya, R. Toyoda, R. Matsuoka, J. F. Kögel, S. Kusaka, K. Hoshiko, T. Yagi, T. Nagayama, H. Nishihara, *J. Mater. Chem. A* **2015**, *3*, 15357-15371; c) A. A. Ali, R. E. Benson, S. Blumentritt, T. S. Cameron, A. Linden, D. Wolstenholme, A. Thompson, *J. Org. Chem.* **2007**, *72*, 4947-4952; d) R. Aoki, R. Toyoda, J. F. Kögel, R. Sakamoto, J. Kumar, Y. Kitagawa, K. Harano, T. Kawai, H. Nishihara, *J. Am. Chem. Soc.* **2017**, *139*, 16024-16027; e) Y. Wang, X. Li, L. Yang, W. Sun, C. Zhu, Y. Cheng, *Mater. Chem. Front.* **2018**, *2*, 554-558. f) H. Ito, H. Sakai, Y. Okayasu, J. Yuasa, T. Mori, T. Hasobe, *Chem. Eur. J.* **2018**, *24*, 16889-16894.
- [8] a) M. Zinic, F. Vogtle, F. Fages, *Top. Curr. Chem.* **2005**, *256*, 39-76; b) J. H. Jung, H. Kobayashi, M. Masuda, T. Shimizu, S. Shinkai, *J. Am. Chem. Soc.* **2001**, *123*, 8785-8789; c) H. Tong, Y. Hong, Y. Dong, Y. Ren, M. Haussler, J. W. Lam, K. S. Wong, B. Z. Tang, *J. Phys. Chem. B* **2007**, *111*, 2000-2007; d) S. Wang, W. Shen, Y. Feng, H. Tian, *Chem. Commun.* **2006**, 1497-1499; e) X. Hou, D. Gao, J. Yan, Y. Ma, K. Liu, Y. Fang, *Langmuir* **2011**, *27*, 12156-12163; f) Y. L. Zhao, I. Aprahamian, A. Trabolsi, N. Erina, J. F. Stoddart, *J. Am. Chem. Soc.* **2008**, *130*, 6348-6350; g) L. J. Chen, B. Jiang, H. B. Yang, *Org. Chem. Front.* **2016**, *3*, 579-587; h) P. Xing, H. P. Tham, P. Li, H. Chen, H. Xiang, Y. Zhao, *Adv. Sci.* **2018**, *5*, 1700552.
- [9] a) B. Yue, L. Yin, W. Zhao, X. Jia, M. Zhu, B. Wu, S. Wu, L. Zhu, *ACS Nano* **2019**, *13*, 12438-12444; b) K. Watanabe, H. Iida, K. Akagi, *Adv. Mater.* **2012**, *24*, 6451-6456; c) X. Gao, X. Qin, X. Yang, Y. Li, P. Duan, *Chem. Commun.* **2019**, *55*, 5914-5917.
- [10] a) J. Han, S. Guo, H. Lu, S. Liu, Q. Zhao, W. Huang, *Adv. Opt. Mater.* **2018**, *6*, 1800538; b) H.-T. Feng, C. Liu, Q. Li, H. Zhang, J. W. Y. Lam, B. Z. Tang, *ACS Mater. Lett.* **2019**, *1*, 192-202; c) H. Tanaka, Y. Inoue, T. Mori, *ChemPhotoChem* **2018**, *2*, 386-402; d) G. Borzsonyi, R. L. Beingessner, T. Yamazaki, J. Y. Cho, A. J. Myles, M. Malac, R. Egerton, M. Kawasaki, K. Ishizuka, A. Kovalenko, H. Fenniri, *J. Am. Chem. Soc.* **2010**, *132*, 15136-15139; e) D. Zheng, L. Zheng, C. Yu, Y. Zhan, Y. Wang, H. Jiang, *Org. Lett.* **2019**, *21*, 2555-2559.
- [11] K. Murata, M. Aoki, T. Suzuki, T. Harada, H. Kawabata, T. Komori, F. Ohseto, K. Ueda, S. Shinkai, *J. Am. Chem. Soc.* **1994**, *116*, 6664-6676.
- [12] D. Niu, Y. Jiang, L. Ji, G. Ouyang, M. Liu, *Angew. Chem. Int. Ed.*, **2019**, *58*, 5946-5950.
- [13] a) H. Wu, B. Wu, X. Yu, P. Zhao, W. Chen, L. Zhu, *Chin. Chem. Lett.* **2017**, *28*, 2151-2154; b) B. Yue, L. Zhu, *Chem. Asian J.* **2019**, *14*, 2172-2180.
- [14] a) A. Ajayaghosh, C. Vijayakumar, R. Varghese, S. J. George, *Angew. Chem. Int. Ed.* **2006**, *45*, 456-460; b) G. Liu, J. Sheng, W. L. Teo, G. Yang, H. Wu, Y. Li, Y. Zhao, *J. Am. Chem. Soc.* **2018**, *140*, 16275-16283; c) Y. Mao, K. Liu, L. Meng, L. Chen, L. Chen, T. Yi, *Soft Matter* **2014**, *10*, 7615-7622; d) P. Xing, Y. Li, Y. Wang, P. Z. Li, H. Chen, S. Z. F. Phua, Y. Zhao, *Angew. Chem. Int. Ed.* **2018**, *57*, 7774-7779.
- [15] J. Zhang, Q. Liu, W. Wu, J. Peng, H. Zhang, F. Song, B. He, X. Wang, H. H. Sung, M. Chen, B. S. Li, S. H. Liu, J. W. Y. Lam, B. Z. Tang, *ACS Nano* **2019**, *13*, 3618-3628.
- [16] a) C. J. Kim, A. Sanchez-Castillo, Z. Ziegler, Y. Ogawa, C. Noguez, J. Park, *Nat. Nanotechnol.* **2016**, *11*, 520-524; b) B. Nowacki, H. Oh, C. Zanlorenzi, H. Jee, A. Baev, P. N. Prasad, L. Akcelrud, *Macromolecules* **2013**, *46*, 7158-7165; c) B. A. San Jose, S. Matsushita, K. Akagi, *J. Am. Chem. Soc.* **2012**, *134*, 19795-19807; d) J. N. Wilson, W. Steffen, T. G. McKenzie, G. Lieser, M. Oda, D. Neher, U. H. Bunz, *J. Am. Chem. Soc.* **2002**, *124*, 6830-6831.
- [17] a) M. R. Craig, P. Jonkheijm, S. C. J. Meskers, A. P. H. J. Schenning, E. W. Meijer, *Adv. Mater.* **2003**, *15*, 1435-1438; b) D. Di Nuzzo, C. Kulkarni, B. Zhao, E. Smolinsky, F. Tassinari, S. C. J. Meskers, R. Naaman, E. W. Meijer, R. H. Friend, *ACS Nano* **2017**, *11*, 12713-12722.

Entry for the Table of Contents (Please choose one layout)

Layout 1:

## RESEARCH ARTICLE

**Split and reunion:** Cholesteryl-linked bis(dipyrrinato)zinc(II) can be employed to construct beads-like nanostructures with mirror-image chiroptical signals. These nanostructures can further undergo a dynamic transformation to a homohelical leaf-like morphology, together with an ON-OFF switch of chiropticity at film state upon external stimuli. The ultra-large optical asymmetry control is in amorphous molecular aggregations.



*Bin Wu, Hongwei Wu, Yunyun Zhou, Dongxiao Zheng, Xiaoyong Jia, Lei Fang, Liangliang Zhu\**

**Page No. – Page No.**

**Controlling Ultra-Large Asymmetry in Amorphous Molecular Aggregations**

Accepted Manuscript